Effect of microwave pulse parameters on energy coupling and enhancement of microwave assisted ignition

Huimin Wu [a,b], Zhaowen Wang [a,b]*, Xiaobei Cheng [a,b], Yuhan Huang [c], Jyh-Yuan Chen [d], Chaohui Liu [a,b], Zhihao Wang [a,b], Jingxing Xu [a,b], Xinhua Zhang [a,b]

[a] *State Key Laboratory of Coal Combustion, Huazhong University of Science and Technology, Wuhan 430074, China*
[b] *School of Energy and Power Engineering, Huazhong University of Science and Technology, Wuhan 430074, China*
[c] *School of Civil and Environmental Engineering, University of Technology Sydney, NSW 2007, Australia*
[d] *Department of Mechanical Engineering, University of California – Berkeley, Berkeley, CA 94720, USA*

Abstract

Microwave Assisted Ignition (MAI) is a promising technology to optimize the lean combustion characteristics of internal combustion engines. This research investigated the effects of microwave pulse waveform and delay time on energy coupling and ignition enhancement by using a power diagnostic with high time-resolution. The pulse width ranged from 80 to 200 μs and the corresponding peak power was adjusted between 1000 and 400 W to keep the incident energy of microwave pulse constant. Results showed that a high power and short width pulse waveform was conducive to the microwave energy absorption. The coupled energy generally decreased with delay time. There was a significant ignition enhancement with only 6~7 mJ energy coupled into the flame kernel, which was approximately 1/5 of total spark energy. Moreover, the ignition enhancement was well correlated with the coupled energy, suggesting that ignition enhancement was determined by coupled energy via electron collision reactions. Finally, the main influencing factor of coupled energy was the energy coupling pattern which changed from none-coupling to saturated coupling. A high pulse power and short delay time facilitated this change. This study revealed the saturated coupling pattern independent of waveform and delay time, which is caused by a stable electron number density due to the cut-off effect.

Keywords: Microwave; Ignition enhancement; Power diagnostic; Energy absorption; Saturated coupling pattern.

*Corresponding author.

Email address:
wangzhaowen1978@163.com;

1. Introduction

Lean combustion is an effective technology to achieve high thermal efficiency and low pollutant emissions for conventional internal combustion engines [1]. However, its main challenges are low ignition rate and slow flame speed. Microwave enhanced plasma [2, 3] is a promising method to overcome these challenges, which has been investigated widely in recent years and demonstrated successful combustion advancements.

Microwave ignition achieves ignition through the synergetic interaction of microwave energy and reaction kinetics [4, 5] and can be divided into two categories. The first category is ignition due to microwave resonance [2, 6], in which the initial microwave plasma generation is relatively harsh. The second category, named microwave assisted ignition (MAI), employs a conventional spark plug to generate an initial ignition kernel and emits microwave to expand the initial spark plasma [3]. Benefiting from its intrinsic high frequency, the microwave energy can be transferred to the electrons directly [7], rather than to the surrounding gas because of particle mass difference. The local gas temperature increment is relatively small. Therefore, the heat loss due to temperature gradient is no longer an issue in MAI [8].

Ikeda et al. [3, 9] invented the first integrated microwave assisted spark plug in 2009, with a light-weight power supply and an easy-to-install discharge unit without modifying the engine combustion chamber. After that, MAI attracted significant research attention. Many engine experiments were conducted subsequently, which revealed significant advantages of MAI, such as decreasing cyclic variation, extending ignition limit [10], extending ignition kernel [11] and reducing unburned hydrocarbon emissions [12]. Visualization experiments in constant volume combustion chambers (CVCC) were carried out subsequently to explore the enhancement mechanism of MAI. Wolk et al. [13] reported that the MAI enhancement mechanism was related to the wrinkle structure on flame surface caused by microwave. Zhang et al. [14] related the ignition enhancement with microwave plasma generation, inferring that the flame wrinkle was mainly the result of a microwave plasma jet effect via temperature gradient and pressure propulsive.

To further improve the ignition performance of MAI, many experiments have been conducted on optimizing the parameters of microwave pulse [15, 16]. However, a wide variety of experiment devices have led to differences in the results. Gu et al. [17] found that the best enhancement was achieved at 10 kHz, while Zhang et al. [18] reported that the MAI enhancement increased with microwave pulse frequency from 1 to 80 kHz. Moreover, Zhang et al. [14] observed that adding 8% CO_2 in air-fuel mixture would cause an opposite effect of microwave pulse frequency on ignition enhancement as that without CO_2. These results have prompted the desire for further understanding the mechanisms of MAI.

Moreover, existing studies usually calculated microwave energy based on stationary power measurement, such as 225 mJ in [13] and 150 mJ in [19]. However, such a rough calculation raises doubt whether MAI is more efficient than spark ignition, considering that the spark energy is typically below 50 mJ. This roughly calculated energy was actually the microwave energy emitted into the CVCC. Only a small proportion of this energy was coupled directly to the electrons in flame kernel, while the remaining energy might be consumed by the CVCC or leaked out from the optical windows, which led to an overestimation of the microwave energy absorbed by flame kernel. Nishiyama et al. [20] transiently measured the absorbed energy on microwave-enhanced laser ignition and indicated that merely 0.5 mJ coupled energy could significantly decrease the minimum ignition energy by about 2 mJ. However, to date, these transient measurements have not been conducted for MAI to determine energy absorption.

To sum up, quantification of the coupled microwave energy is critical to demonstrate the advantages of MAI and to further understand the enhancement mechanism in the aspect of energy deposition. Therefore, in this study, the microwave energy directly coupled into ignition kernel is measured by a high-time-resolution power diagnostic to evaluate the advantages of MAI. The effect of microwave pulse on coupled energy is investigated to optimize microwave parameters (i.e. pulse waveform and delay time). Meanwhile, the ignition enhancement is correlated with the coupled energy to explore the microwave enhancement mechanism. Finally, the main influencing factor of coupled energy efficiency is elaborated.

2. Experimental setup and diagnostics

2.1 MAI device

The experimental setup is modified from that described in [14] and briefly summarized here. The experiments were performed in a CVCC, as sketched in Fig. 1. A premix tank was adopted to ensure a fixed equivalent ratio of 0.7 for the methane-air mixture. The combustion chamber was pressurized to an absolute pressure of 0.2 MPa before the experiment. A straight type Schlieren system was employed to image ignition kernel, using two f=700 mm convex lenses to collimate and refocus light and a knife edge. In addition, a back-light method with a microscopic lens (QM-1 Questar) was used to photograph the luminous plasma zone. Images were recorded at 40,000 frames per second with 25 μs exposure time. A solid-state microwave source generating 2.45 GHz microwave was connected to an antenna. The antenna was developed based on an N-J type coaxial connector and was placed opposite to a spark plug. The center electrode of spark plug was elongated. The pin-to-pin

electrodes configuration was favorable for ignition kernel expansion. The signal generator (TFG-VII Fastlaser Tech) issued three transistor-transistor logic (TTL) signals to trigger the high-speed camera, spark coil and microwave source. The time intervals between the three TTL signals can be adjusted to fit experimental purposes. As shown in Fig. 2, the camera was started 1 ms before the spark plug. The signals interval between spark coil and microwave source was defined as the delay time (DT).

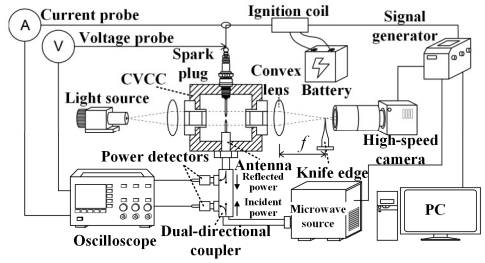

Fig. 1. Experiment setup.

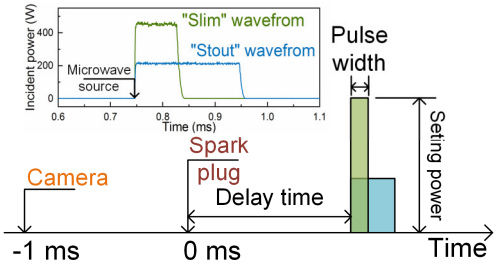

Fig. 2. Sketch of three TTL signals and the measured pulse waveforms.

Table 1
Waveform configurations

Waveform*	Setting power (W)	Pulse width (μs)
PW 80	1000	80
PW 100	800	100
PW 120	667	120
PW 160	500	160
PW 200	400	200

*In the absence of ignition, the incident energy is constant at various waveforms.

In this study, only one microwave pulse was emitted after ignition to reduce interference. Incident power means the power emitted from microwave source to internal CVCC and reflected power means the power reflected from CVCC to microwave source. The pulse waveform had adjustable pulse width and incident power. The incident microwave energy was kept constant to estimate the absorption efficiency of microwave energy under various waveforms. As shown in Fig. 2, the measured pulse waveform is a square wave. The "slim" waveform has high peak power and short pulse width, while the "stout" waveform has low peak power and long pulse width. We use the value of the pulse width (PW) to distinguish the pulse waveform. The pulse waveforms investigated in this study are presented in Table 1.

2.2 Electrical measurement of ignition circuit and power diagnostic of microwave

Electrical measurement of ignition circuit was achieved by a high-voltage probe (P6015A Tektronix) and a current probe (TCP 312 Tektronix) to detect the discharge voltage and current, respectively. The voltage probe was inserted into the high-voltage cable that connected the ignition coil and spark plug. The ground clip of voltage probe was contacted with the center electrode of the antenna. The current probe was clamped outside of the high-voltage cable and the current data was pre-processed by an amplifier (TCPA 300 Tektronix) with 3% accuracy. The electrical data were recorded by an oscilloscope (MDO 3024 Tektronix) with a time resolution of 4 ns. The ignition energy was calculated by the measured voltage and current. The charging time of the ignition coil was fixed at 3 ms, and the ignition energy of the spark plug is constant at approximately 34±3 mJ under all experimental conditions.

The microwave power diagnostic measured the incident and reflected power, which included two power detectors (EZM2040N Eclipse MDI) mounted on a dual-directional coupler (Narda 3022, 20 dB attenuation). The power data were also recorded by the same oscilloscope. Since the unit of raw data from power detectors was volt, a calibration from volt to watt was conducted without spark ignition using a ten-second microwave pulse. During the calibration, the corresponding power values (dBm) are obtained by two low-frequency power meters (KC 9531). Fig. 3 shows the calibration curve.

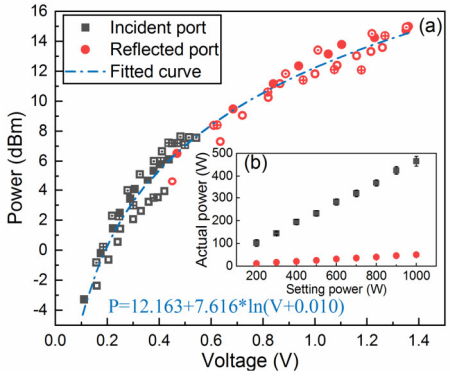

Fig. 3. (a) Voltage-power calibrated curve and (b) comparison between the setting power of microwave source and the actual power during calibration.

To separate the incident and reflected powers, attenuations of 30 dB and 10 dB were mounted in the incident and reflected ports, respectively. The

calibration curve shows a good logarithmic fitting between the voltages (V) and powers (P) of P=12.163+7.616×ln(V+0.010) [dBm]. It should be noted that all the transient powers in this article were first calculated to decibel-milliwatt (dBm) from the measured voltages through this calibration curve. It is then converted to milliwatt units by P '=10^(P/10) [mW] after considering the attenuations. Fig. 3 (b) shows the calibrated actual power (incident and reflected) into the CVCC versus the setting power during calibration. The incident power is 45% of the setting power under all power conditions. Similar low transmission efficiencies are common in previous studies [13, 21], which is caused by the incomplete impedance matching between the transmission components [21]. Although there is a difference between the incident and actual powers, the linear relationship between them still ensures a constant incident energy in various waveforms listed in Table 1. Moreover, the reflected power was approximately 10% of the incident power in all conditions, which indicated that 90% of the incident power is consumed by the CVCC.

2.3 Coupled microwave energy

Four microwave pulses are sequentially emitted after ignition to illustrate how the plasma energy is coupled. Fig. 4 shows the effect of these four pulses on the incident and reflected powers. The waveforms of these four pulses are identical, with 900 W setting power and 0.2 ms pulse width. The corresponding plasma micrographs of each pulse are presented at the top and the transient powers without ignition are plotted in black line for comparison. The first two pulses lead to microwave plasma generation, while the last two pulses do not. Although the setting power is the same, the measured incident power increases from 400 to 450 W with microwave plasma generation. It means that microwave plasma will lead to an increase in the transmission efficiency of the MAI system. This may be because an additional load, i.e. plasma, occurs in the transmission line, which relieves the incomplete impedance matching [22]. Meantime, the occurrence of plasma led to a drop in reflected power from 40 to 20 W. Therefore, microwave energy coupling is caused by plasma generation.

The discrepancy between incident and reflected energies represents the energy deposited in CVCC, which mainly includes the energy loss by the interior structure of CVCC (E_{loss}) and the energy coupled by ignition kernel (it is naught in the none-plasma case, such as pulse 3 in Fig. 4). The value of E_{loss} depends on the interior structure of CVCC and the incident energy, which is precalculated in the none-plasma case. The calculation of E_{loss} is constant at 37.6±4 mJ under all experimental conditions, due to the constant incident energy and CVCC structure. In the case of microwave plasma generation, the discrepancy between incident and reflected energies minus E_{loss} is the energy coupled by ignition kernel, which is described by the following equation:

$$E_{coupled} = \int_{t_1}^{t_2}(P_{inc} - P_{ref})dt - E_{loss} \ , \quad (1)$$

where $E_{coupled}$ is the coupled energy, P_{inc} and P_{ref} are the incident and reflected powers, respectively. t_1 and t_2 are the microwave emitted and expired time. In Fig. 4, the coupled energy is shown as the sum of the increased incident energy (marked by blue) and the reduced reflected energy (marked by green).

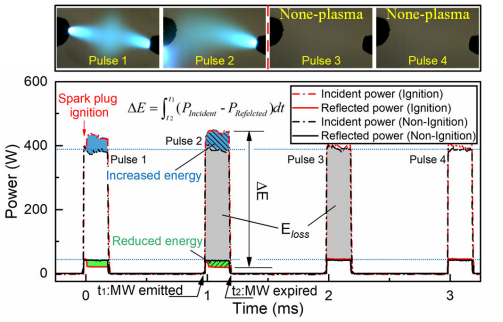

Fig. 4. Comparison of transient powers between plasma generation and none-plasma cases at four pulses.

2.4 Flame enhancement index

In previous research [13, 17], the average size of ignition kernel was used to estimate the ignition enhancement of MAI. However, the "plasma jet" found in [14] implied that the ignition enhancement does not exist in all directions. The average size makes the enhancement effect diluted. Therefore, we defined an enhancement index (EI) of flame velocity at eight special directions to properly estimate the ignition enhancement. These directions are marked per 45 degrees in clockwise from 1st to 8th (i.e. V1 to V8), as shown in Fig. 5 (a). The flame velocity at each direction was defined as the distance that the flame front advanced per unit time. EI is calculated using equation (2):

$$\mathrm{EI}=1/8 * \sum_{i=1}^{8} \int (v_{\mathrm{MAI,i}} - v_{\mathrm{SI,i}})/(v_{\mathrm{SI,i}})\mathrm{dt} \ , \quad (2)$$

where $v_{\mathrm{MAI,i}}$ is the velocity in the i^{th} direction under MAI case, and $v_{\mathrm{SI,i}}$ is the average of that in seven repeated spark ignition (SI) cases to reduce the factor of random SI events. Fig. 5 (b) shows the flame velocities under SI and MAI cases. The flame velocity increased rapidly to 9 m/s at 0 ms because of spark ignition under both MAI and SI. Then the flame speed in SI decreased and stabilized at 0.6 m/s. When the microwave was emitted at 0.5 ms under MAI, the flame speed was increased to 9 m/s again, resulting in an obvious ignition enhancement in the 4th direction as shown in Fig. 5 (a). If the direction of ignition enhancement is not perpendicular to the Schlieren parallel light, EI will be underestimated. To reduce

this uncertainty, the experiment is repeated at least five times.

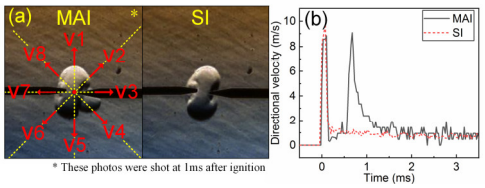

Fig. 5. (a) Definition of enhancement index and (b) comparison of flame velocities between MAI and SI at the 4th direction.

3. Results and discussion

3.1 Effect of microwave pulse parameters on ignition enhancement

In this section, the ignition enhancement by microwave pulse is investigated at various pulse waveforms and delay time. The enhancement index (EI), which represents the average velocity enhancement in the eight directions, is used to estimate ignition enhancement.

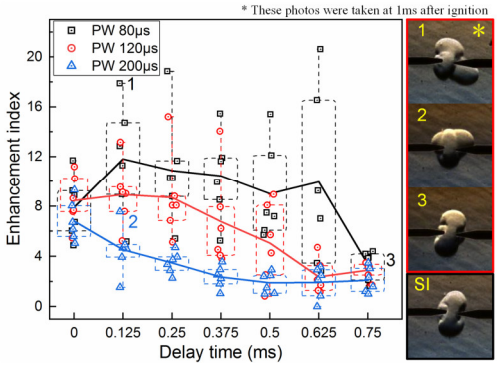

Fig. 6. Ignition EI of different microwave pulse waveforms. The solid lines represent the average of EI. The dash line boxplots (25th and 75th percentiles, box; minimum and maximum, whiskers) show the data distribution of repeated experiments for each condition.

Fig. 6 illustrates the effect of microwave pulse waveform and delay time on EI. Three typical points are selected and the corresponding kernel images are presented on the right to clarify ignition enhancement. SI image is also shown for comparison. Fig. 6 shows that a slimmer waveform, i.e., high power and short pulse width, induces a larger EI. The EI of PW 200 is generally lower than that of PW 120. The EI of PW 80 is relatively highest, with some EI values even exceeding 16, which indicates a significant enhancement. The ignition kernel image shows similar results. The kernel size of PW 80 (image 1) is significantly larger and the flame front propagates further than that of PW 200 (image 2). In addition, a small delay time about 0.125 ms increases EI slightly to the peak at PW 80 and PW 120 case. However, the EI generally decreases with delay time. When the delay time is over 0.625 ms, the EI drops to only 2 and the effect of pulse width becomes negligible. As shown in image 3 (DT=0.75 ms, PW=80 μs), the shape and size of ignition kernel are very similar to that of SI, indicating no ignition enhancement.

In general, Fig. 6 demonstrates that a high power and short width pulse waveform and a delay time of 0.125 ms facilitate the ignition enhancement.

3.2 Effect of microwave pulse parameters on microwave energy absorption

Although the microwave energy emitted to the CVCC is fixed in our experiment, the coupled energy might be different. In this section, the energy coupled by ignition kernel is calculated to optimize the microwave pulse parameters. Additionally, the EI is correlated with the coupled energy to explore the microwave enhancement mechanism.

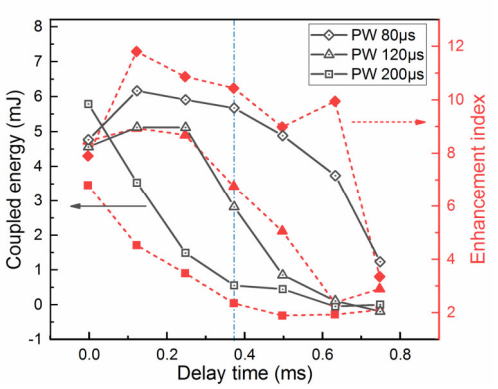

Fig. 7. Comparison of coupled energy and ignition enhancement index.

Fig. 7 shows the effect of microwave pulse parameters on energy absorption. The maximum energy coupled by ignition kernel is among 6~7 mJ, which is approximately 1/5 of the spark energy (34 mJ). Interestingly, the effect of pulse waveform on coupled energy is similar to that on the EI. A slimmer pulse waveform induces a larger coupled energy. For example, PW 80 and PW 120 contribute 5.67 and 2.81 mJ of coupled energy at 0.375 ms delay time, respectively, while the coupled energy at PW 200 approaches 0 mJ. In addition, an excessive delay time inhibits the coupling of microwave energy. The coupled energy reaches the peak with a minor delay time of 0.1~0.3 ms in PW 80 and PW 120. When the delay time exceeds 0.5 ms, the coupled energy diminishes to 0 mJ.

The almost identical tendencies of coupled energy and EI imply that the ignition enhancement is correlated to the coupled energy. However, the microwave energy, as an electromagnetic energy, cannot directly enhance the macroscopic ignition

event. Hence, electron collision is a plausible explanation correlating the coupled energy and ignition enhancement. The lightest electrons absorb a large amount of microwave energy [23], which causes the electrons to easily accelerate and deflect in microwave field. The energetic electrons then transfer energy to the gas molecules through collisions. The molecules are excited or dissociated into radicals and the temperature of plasma zone is also escalated [15]. Localized overheating in the plasma zone propels the momentum and radical particles to the front of ignition kernel, resulting in ignition enhancement. Fig. 8 explains this phenomenon. If the flame propagation is rapid enough, this "plasma jet" could not catch up with the flame front, which explains why the enhancement is diminished under near-stoichiometric conditions [13].

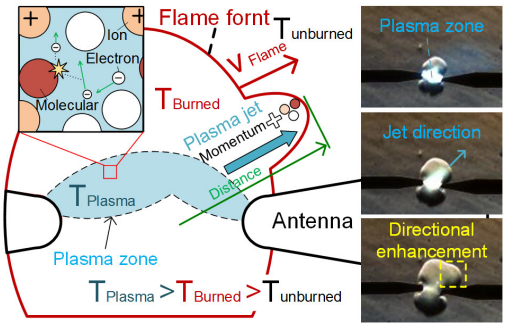

Fig. 8. Energy transfer from electrons to gas and directional enhancement of microwave plasma.

3.3 Essence of microwave energy absorption

In this section, the transient energy of microwave is calculated to investigate the essence of microwave energy coupling.

Fig. 9 shows the relationship between the incident and reflected microwave energies at different pulse waveforms. For lower power and larger pulse width cases, such as PW 200 and PW 160, the reflected energy increases linearly with the incident energy. The corresponding kernel images show neither microwave plasma nor ignition enhancement. As the peak power increases, the energy curve deviates towards the axis of incident energy, such as PW 100. The kernel images show obvious microwave plasma and ignition enhancement. Therefore, the linear relationship suggests that microwave energy cannot be absorbed and the overlap of PW 200 and 160 is contributed from the identical energy loss by the CVCC structure (E_{loss}). Once the microwave plasma generates, the abundant electrons in plasma continuously absorb microwave energy. Consequently, the energy curve deviates toward the incident energy axis. The discrepancy between curved and linear energies is the microwave energy coupled into electrons. Therefore, the efficiency of energy coupling depends on two factors: 1) the threshold where the energy curve begins to deviate; and 2) the slope of the energy curve. As one of the factors, the absorption threshold decreases with the waveform getting slimmer, which is 11.9, 7.5, 2.7 mJ in PW 120, 100 and 80, respectively. However, in some lower power cases, energy absorption does not occur even for long pulse durations, such as PW 200. This indicates that a larger incident power favors the generation of microwave plasma, because the pulse duration hardly affects the energy threshold and absorption efficiency.

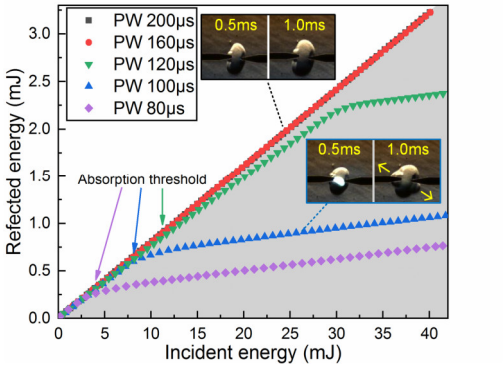

Fig. 9. Relationship of the incident and reflected energies under various pulse waveforms at 0.5 ms delay time.

As another factor, the slopes of the incident and reflected energies curves at various pulse waveforms and delay times are investigated and plotted in Fig. 10. Two slopes are worth mentioning: the first one is about 8.0×10^{-2} labeled by the gray zone (K_1), which is the initial slope value, and the second value is about 1.3×10^{-2} labeled by the pink zone (K_2), which is the finally converged slope in most plasma generation cases. The first slope value represents no microwave energy being absorbed, since microwave plasma cannot be generated immediately with the microwave emission. This hypothesis is verified by the non-plasma cases, such as PW 200, where the slope almost keeps constant at K_1. Because a constant slope implies a stable energy coupling pattern, the second slope value reveals a surprising phenomenon that the energy coupling is saturated eventually in most plasma generation cases. The saturated energy coupling is irrelevant to waveform and delay time. In summary, the K_1 and K_2 represent the none-coupling and saturated-coupling patterns, respectively. Therefore, the period of switching between these two patterns significantly affects the absorption efficiency of microwave energy. This period decreases with the increase of incident power, as shown in Fig. 10 (a). The period to achieve the saturated-absorption is 0.10 ms in PW 120, which is almost 5/6 of the pulse width, while it is only 3/10 in PW 100 and 1/4 in PW 80. It is obvious that a larger incident power promotes the absorption efficiency. Moreover, as presented in Fig. 10 (b), the period increases with delay time, except for the DT 0 ms case. As the delay time rises from DT

0.125 ms to DT 0.625 ms, the period increases from 0.0072 ms to 0.0624 ms. In summary, the absorption efficiency decreases with delay time.

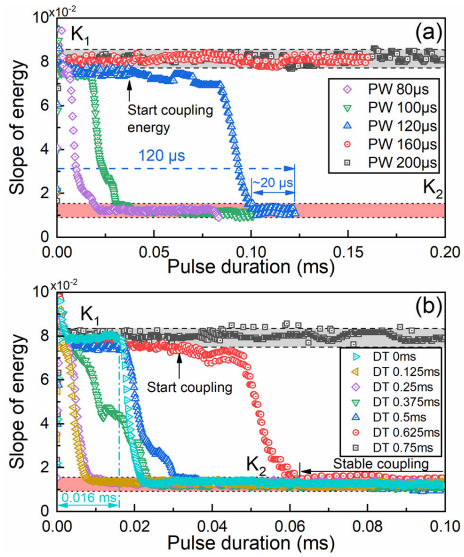

Fig. 10. Slopes of the incident and reflected energies curve in (a) various pulse widths at 0.5 ms delay time and (b) various delay times at 100 μs pulse width.

Although a saturated coupling pattern independent of microwave parameters is found, it is still unclear about its causes. In the following, the cause of the saturation coupling pattern will be analyzed in terms of the plasma electrical properties.

The microwave power absorbed per unit volume of the plasma (W_{ab}) can be described using equation (3) [24]:

$$W_{ab}=A n_e \mu_e E^2 \quad , \qquad (3)$$

where μ_e is the mobility of the electrons, n_e is the electron number density, E is the electric field of microwave and the quantity A is assumed as 1 for simplicity. The electron mobility μ_e is approximated as a constant value under our experimental conditions [25]. Moreover, the spatial microwave field is proportional to the square root of incident power ($P^{1/2}$) [26]. So E^2 can be approximated as a positive correlation with the incident power P. Therefore, the absorbed power of ignition kernel strongly depends on the electron number density and incident power. Thus, the constant value of the energy slope in Fig. 10 may be caused by the stabilization of electron number density in plasma. In this study, electrical measurement was employed simultaneously to detect the plasma properties. The electron number density is calculated using equation (4) [27], in which the number density is related to plasma resistance:

$$n_e=\upsilon\, m_e I L / e^2 V S, \qquad (4)$$

where I and V is the current and voltage during MAI, respectively, obtained from electrical measurement; the geometric parameters L and S are the visual length and cross-sectional area, respectively, determined from the micrographics shown in Fig. 11 (c); υ is the electron-gas collision frequency, m_e and e are the electron mass and elementary charge, respectively [27]. Fig. 11 presents the calculation of electron density. The electron number density remains constant at 3.1×10^{15}cm^{-3} when microwave plasma is generated, and this value is independent of the microwave parameters. It should be mentioned that the values of number density deviated from the red dotted line (3.1×10^{15} cm^{-3}) are inaccurate because it is difficult to identify the plasma cross-sectional area (S) in the absence of luminous plasma. It may be the reason for the slightly lower electron density at large delay time cases, such as DT 0.5 ms. Importantly, the electron density barely changes in the none-coupling case, such as PW 200, implying that the plasma is not generated. The "cut-off" effect of plasma [17] is a reasonable explanation for the stable electron density: microwave propagation is blocked by the plasma with high electron density. This effect can be neglected as the electron density is below a certain level. Thus, the trade-off between microwave coupling and blocking keeps the electron number density constant.

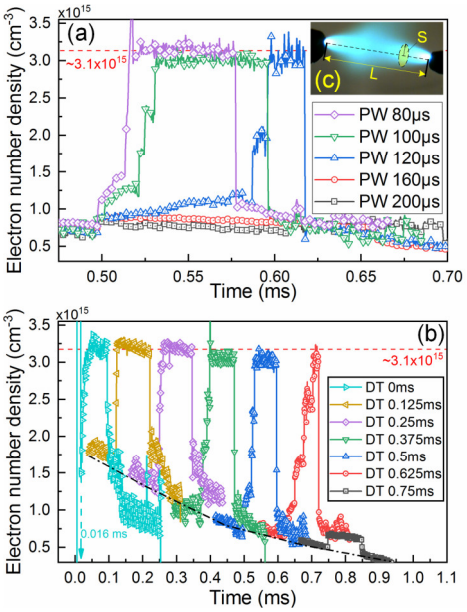

Fig. 11. Variation of electron number density at (a) various pulse width and (b) various delay time. (c) Definition of the geometric parameters L and S.

Based on the above coupling mechanism of MAI, the difference of coupled energy among various microwave parameters can be explained. The incident

power of the slim waveform is enormous, such as PW 80. The microwave field strength is significant correspondingly, which is conducive to abundant energetic electrons. These energetic electrons enhance gas reactions and generate additional electrons via collision reactions. The electron number density escalates rapidly, which benefits the generation of microwave plasma. Consequently, the saturated coupling pattern is achieved in a short period and the absorption efficiency is obviously higher. As for the effect of delay time, the electron density gradually drops to about 10^7 cm^{-3} after spark ignition [17], this tendency is shown as the black dotted line in Fig. 11 (b). A longer delay time leads to fewer free electrons to participate in collision reactions, and the plasma generation is hindered. Therefore, the absorption efficiency decreases with delay time. Moreover, the cut-off effect is thought as the culprit of the anomaly at DT 0 ms, where the absorption efficiency is lower than that of DT 0.25 ms. An electron density of 10^{17} cm^{-3} right after ignition has been reported in [28] which is much larger than the constant value of 3.1×10^{15} cm^{-3}. Thus, most of the microwave energy is blocked and the absorption efficiency is limited. It was not until ~0.016 ms that the electron density falls down to the constant value, energy absorption begins, and the microwave plasma is established immediately.

4. Conclusions

Power diagnostic with high-time-resolution was employed in MAI to measure the microwave energy coupled by ignition kernel. The effects of microwave pulse waveform and delay time on ignition enhancement and energy coupling were investigated. The main conclusions are summarized as follows:

1. With a fixed incident energy, a higher power and shorter pulse width waveform facilitates the ignition enhancement and coupled energy.
2. A slight delay of microwave emission (0.1-0.3 ms) is the optimal for energy coupling.
3. A mere 6~7 mJ of coupled microwave energy, about 1/5 of the total spark energy, results in a significant ignition enhancement.
4. The ignition enhancement is directly related to the coupled energy. The coupled energy is transferred to the macroscopic ignition enhancement via electron collision reactions.
5. The saturated coupling pattern resulted from a stable electron number density is found. The transition from none-coupling to saturated-coupling pattern affects the efficiency of energy coupling.

Overall, the power diagnostic presented here is essential for better understanding of the ignition enhancement in MAI. This diagnostic enables further exploration of other parameters affecting the microwave energy coupling. Particularly, the discovery of the saturated coupling pattern suggests that future research can focus on optimizing the microwave frequency to increase the saturated value of electron density for higher microwave absorption efficiency.

Acknowledgements

This work was supported by the National Natural Science Foundation of China (Grant number 51576083). The assistance of Junhui Cao in the image processing is greatly appreciated.

References

[1] J.A. Caton, A comparison of lean operation and exhaust gas recirculation: thermodynamic reasons for the increases of efficiency, Report No. 0148-7191, SAE Technical Paper, 2013.
[2] M.K. Le, A. Nishiyama, Y. Ikeda, Evaluation of a novel miniaturised microwave resonating igniter: The Flat Panel Igniter, Proceedings of the Combustion Institute 37 (2019) 5613-5620.
[3] Y. Ikeda, A. Nishiyama, Y. Wachi, M. Kaneko, Research and development of microwave plasma combustion engine (Part I: concept of plasma combustion and plasma generation technique), Report No. 0148-7191, SAE Technical Paper, 2009.
[4] Y. Ju, W. Sun, Plasma assisted combustion: Dynamics and chemistry, Progress in Energy and Combustion Science 48 (2015) 21-83.
[5] A. Starikovskiy, N. Aleksandrov, Plasma-assisted ignition and combustion, Progress in Energy and Combustion Science 39 (2013) 61-110.
[6] Z. Wang, J. Huang, Q. Wang, L. Hou, G. Zhang, Experimental study of microwave resonance plasma ignition of methane–air mixture in a constant volume cylinder, Combustion and Flame 162 (2015) 2561-2568.
[7] Z. Wang, J. Li, B. Li, Q. Nie, Z. Zhang, A. Mao, Energy absorption effects of the electromagnetic waves in collisional dusty plasmas, AIP Advances 9 (2019) 115205.
[8] Y. Ikeda, Development of 2.45 GHz Semiconductor Microwave System for Combustion Ignition Enhancement and Failure Analysis, Materials (Basel) 15 (2022).
[9] Y. Ikeda, A. Nishiyama, H. Katano, M. Kaneko, H. Jeong, Research and development of microwave plasma combustion engine (Part II: engine performance of plasma combustion engine), Report No. 0148-7191, SAE Technical Paper, 2009.
[10] A. DeFilippo, S. Saxena, V. Rapp, R. Dibble, J.-Y. Chen, A. Nishiyama, Y. Ikeda, Extending the lean stability limits of gasoline using a microwave-assisted spark plug, Report No. 0148-7191, SAE Technical Paper, 2011.
[11] J. Hwang, W. Kim, C. Bae, Influence of plasma-assisted ignition on flame propagation and performance in a spark-ignition engine, Applications in Energy and Combustion Science 6 (2021) 100029.
[12] V.H. Rapp, A. DeFilippo, S. Saxena, J.-Y. Chen, R.W. Dibble, A. Nishiyama, A. Moon, Y. Ikeda, Extending lean operating limit and reducing emissions of methane spark-ignited engines using a microwave-assisted spark plug, Journal of Combustion 2012 (2012).
[13] B. Wolk, A. DeFilippo, J.-Y. Chen, R. Dibble, A. Nishiyama, Y. Ikeda, Enhancement of flame development by microwave-assisted spark ignition in constant volume combustion chamber, Combustion and Flame 160 (2013) 1225-1234.

[14] X. Zhang, Z. Wang, H. Wu, C. Liu, X. Cheng, J.-Y. Chen, Propulsive effect of microwave-induced plasma jet on spark ignition of CO2-diluted CH4-air mixture, Combustion and Flame 229 (2021) 111400.
[15] P. Kumar, Y. Yamaki, J. Lee, S. Nakaya, M. Tsue, Effects of microwave radiation on laser induced plasma ignition of n-butane/air mixture under atmospheric conditions, Proceedings of the Combustion Institute 38 (2021) 6593-6603.
[16] X. Cheng, X. Zhang, Z. Wang, H. Wu, Z. Wang, J.-Y. Chen, Effect of Microwave Pulses on the Morphology and Development of Spark-Ignited Flame Kernel, Energies 14 (2021) 6205.
[17] X. Gu, H. Shiono, S. Nakaya, M. Tsue, Ignition performance of pulsed microwave-assisted sparks in lean methane/air mixture, (2015).
[18] X. Zhang, Z. Wang, H. Wu, D. Zhou, S. Huang, X. Cheng, J.-Y. Chen, Experimental study of microwave assisted spark ignition on expanding C2H2-Air spherical flames, Combustion and Flame 222 (2020) 111-122.
[19] X. Zhang, Z. Wang, D. Zhou, H. Wu, X. Cheng, B. Jin, J.-Y. Chen, Strengthening effect of microwave on spark ignited spherical expanding flames of methane-air mixture, Energy Conversion and Management 224 (2020) 113368.
[20] A. Nishiyama, A. Moon, Y. Ikeda, J. Hayashi, F. Akamatsu, Ignition characteristics of methane/air premixed mixture by microwave-enhanced laser-induced breakdown plasma, Optics express 21 (2013) A1094-A1101.
[21] J. Hwang, C. Bae, J. Park, W. Choe, J. Cha, S. Woo, Microwave-assisted plasma ignition in a constant volume combustion chamber, Combustion and Flame 167 (2016) 86-96.
[22] S. Lee, W. Nam, J. Lee, G. Yun, In situ impedance measurement of microwave atmospheric pressure plasma, Plasma Sources Science and Technology 26 (2017) 045004.
[23] J. Hwang, W. Kim, C. Bae, W. Choe, J. Cha, S. Woo, Application of a novel microwave-assisted plasma ignition system in a direct injection gasoline engine, Applied Energy 205 (2017) 562-576.
[24] E. Karoulina, Y.A. Lebedev, The influence of the electron transport cross sectional shape on electron energy distribution functions in DC and microwave plasmas, Journal of Physics D: Applied Physics 21 (1988) 411.
[25] A. Tejero-del-Caz, V. Guerra, D. Gonçalves, M.L. da Silva, L. Marques, N. Pinhao, C. Pintassilgo, L. Alves, The LisbOn KInetics Boltzmann solver, Plasma Sources Science and Technology 28 (2019) 043001.
[26] Q. Wang, G. Zhang, Y. Liu, L. Hou, C. Liu, Z. Wang, J. Huang, Visual features of microwave ignition of methane-air mixture in a constant volume cylinder, Applied Physics Letters 103 (2013) 204104.
[27] D.Z. Pai, D.A. Lacoste, C.O. Laux, Nanosecond repetitively pulsed discharges in air at atmospheric pressure—the spark regime, Plasma Sources Science and Technology 19 (2010) 065015.
[28] C.A. Bye, A. Scheeline, Stark electron density mapping in the high voltage spark discharge, Spectrochimica Acta Part B: Atomic Spectroscopy 48 (1993) 1593-1605.